RSC Advances

PAPER

View Article Online
View Journal | View Issue

Cite this: *RSC Adv.*, 2024, **14**, 20561

The highly selective green colorimetric detection of yttrium ions in biological and environmental samples using the synergistic effect in an optical sensor

Mahmood D. Aljabri,[a] Salah M. El-Bahy,[b] Refat El-Sayed,[ac] Khaled F. Debbabi[ad] and Alaa S. Amin *[c]

A new eco-friendly method for creating an optical sensor membrane specifically designed to detect yttrium ions (Y^{3+}) has been developed. The proposed sensor membrane is fabricated by integrating 4-(2-arsonophenylazo) salicylic acid (APASA), sodium tetraphenylborate (Na-TPB), and tri-*n*-octyl phosphine oxide (TOPO) into a plasticized poly(vinyl chloride) matrix with dimethyl sebacate (DMS) as the plasticizer. In this sensor membrane, APASA functions dually as an ionophore and a chromoionophore, while TOPO enhances the complexation of Y^{3+} ions with APASA. The composition of the sensor membrane has been meticulously optimized to achieve peak performance. The current membrane exhibits a linear dynamic range for Y^{3+} ions from 8.0×10^{-9} to 2.3×10^{-5} M, with detection and quantification limits of 2.3×10^{-9} and 7.7×10^{-9} M, respectively. No interference from other potentially interfering cations and anions was observed in the determination of Y^{3+}. The membrane showed strong stability and a swift response time of about 3.0 minutes, with no signs of APASA leaching. This sensor is highly selective for Y^{3+} ions and can be renewed by treating it with 0.15 M HNO_3. It has been effectively applied to measure Y^{3+} in nickel-based alloys, as well as in biological and environmental samples.

Received 25th May 2024
Accepted 22nd June 2024

DOI: 10.1039/d4ra03854a

rsc.li/rsc-advances

Introduction

Rare earth elements (REEs), such as yttrium, are crucial for numerous technological advancements and are considered essential due to their extensive applications in various technologies.[1,2] Yttrium, a rare earth ion,[3] is relatively dispersed in nature.[4] It is primarily sourced from three main minerals: xenotime, monazite, and bastnaesite.[5] Over the past thirty years, yttrium has been utilized in numerous fields,[6] including fluorescent materials,[7] catalysis,[8] nanomaterial synthesis[9,10] and targeted radiotherapy,[11] and as a model surface for studying DNA hybridization.[12] Nevertheless, the increasing use of Y^{3+} has raised concerns, as it is highly toxic to living organisms[13] and contributes to radioactive waste, leading to environmental pollution.[14] The purity of yttrium must be meticulously controlled to meet the high standards of industrial applications. Yttrium often coexists with other rare earth elements (REEs) in rare earth ores.[15–17] Consequently, the separation of yttrium from these ores is both necessary and crucial. Among the various methods for purification and separation, solvent extraction is recognized as one of the most efficient techniques.[17–21] Numerous extraction systems have been developed for this purpose, including neutral phosphorus extractants,[22] carboxylic acids,[23,24] phosphorus acids,[25] and amines.[26] Currently, carboxylic acid extraction systems are the most commonly used for separating Y^{3+} from leaching solutions of rare earth ores.[17,23]

Determining Y^{3+} in biological and environmental samples is crucial. Traditional methods for measuring yttrium(III) include inductively coupled plasma atomic emission spectrometry (ICP-AES),[27,28] graphite furnace atomic absorption spectrometry,[29] inductively coupled plasma mass spectrometry (ICP-MS),[2,30] flame atomic absorption spectrometry (FAAS),[31] energy-dispersive X-ray spectroscopy (EDX),[32] laser-induced breakdown spectroscopy (LIBS),[33] X-ray fluorescence,[34] and fluorescence sensors.[4,35] However, these methods often require sophisticated and costly instruments that may not be accessible in all laboratories. Additionally, commonly used spectrophotometric methods[5,14,36–38] for Y^{3+} quantification, which involve complexation, tend to be either expensive or involve complicated fabrication procedures. Hence, it became imperative to pursue a swift, precise, and user-friendly technique for

[a]*Department of Chemistry, University College in Al-Jamoum, Umm Al-Qura University, 21955 Makkah, Saudi Arabia*

[b]*Department of Chemistry, Turabah University College, Taif University, Taif, Saudi Arabia*

[c]*Chemistry Department, Faculty of Science, Benha University, Benha, Egypt. E-mail: asamin2005@hotmail.com*

[d]*Department of Chemistry, High Institute of Applied Science & Technology of Monastir, Monastir, Tunisia*

detecting Y^{3+}. In contrast to traditional detection methods,[39,40] optical chemical sensors have garnered substantial attention from researchers due to their specificity, precision, affordability, instantaneous response, and simplicity.[41–49] As a result, there is an urgent need to develop an optical sensor that is facile to fabricate and adept at identifying Y^{3+}. To our knowledge, this study marks the inaugural documentation of a highly sensitive colorimetric method for detecting and quantifying Y^{3+} using an optical sensor.

The novelty of the present investigation, is to prepare a plasticized PVC membrane immobilizing 4-(2-arsonophenylazo)salicylic acid (APASA) and employed to craft an ion-selective sensor aimed to determine Y^{3+} ions. The main challenge faced was the slow reaction rate between Y^{3+} and APASA. Overcoming this hurdle involved introducing an additional reagent, such as tri-*n*-octyl phosphine oxide (TOPO), to enhance the complexation of Y^{3+} by APASA within the membrane. It is worth noting that there is scarce literature[50–54] on this method, which explores the use of synergistic effects in constructing optical sensors, based on our current knowledge. Additionally, the APASA membrane was applied to detect Y^{3+} in spiked samples, including genuine water samples from various sources and fetal bovine serum, yielding satisfactory and meaningful results.

Experimental

Reagents

All chemicals and reagents used were of analytical reagent quality and used without any further refinement. The experiments employed deionized water. Substances such as high molecular weight PVC, diethyl sebacate (DES), dibutyl phthalate (DBP), dimethyl sebacate (DMS), tri-octyl phosphine oxide (TOPO), sodium tetraphenyl borate Na-TPB *o*-nitrophenyl octyl ether (*o*-NPOE), and tetrahydrofurane (THF) were sourced from Merck or Fulka Chemical Companies and utilized as received. A borate buffer, previously prepared and with a pH range spanning from 5.65 to 10.50, was used to maintain a stable pH in the solutions.[55]

To prepare a standard Y^{3+} solution, 0.0635 g of pure Y_2O_3 was dissolved in 25 mL of dil. HNO_3 (1 part nitric acid to 4 parts water), and the solution was subsequently diluted to a final volume of 500 mL in a calibrated flask. From this solution, a 50 mL portion was transferred into a 500 mL calibrated flask and diluted to the mark, resulting in a solution where 1.0 mL contained 10 μg of yttrium. Subsequent to this, working standard solutions were created by appropriately diluting the stock solutions. The preparation and purification of the reagent (APASA) were conducted according to the methodology outlined in our previous investigation.[56]

Apparatus

Deionized water was created using a Fisons (UK) dual glass distillation apparatus. For spectroscopic analyses, a JASCO 530V UV-Vis spectrophotometer was employed. Y^{3+} ion determination was conducted *via* ICP-AES (PerkinElmer, Germany, 8300). In absorption studies, thin films were positioned within a quartz cuvette, and all measurements were conducted at 25 ± 2 °C in a batch configuration. pH measurements were measured using a Jenway 3505 pH meter (powered by 9 V-AC).

Crafting the sensor membrane

The membrane formation process involved mixing 30 mg of PVC, 60 mg of DMS plasticizer, and 4.0 mg of APASA. Additionally, varying quantities of Na-TPB and TOPO (*e.g.*, 2.0 mg Na-TPB and 4.0 mg TOPO) were added to this mixture if required. The membrane materials were completely dissolved in 1.0 mL of THF. A 100 μL aliquot of this THF solution was then taken and spread onto a glass plate. Prior to application, all glass plates were meticulously cleaned with pure THF to remove any organic residues and dust particles.

After being spun for 2.0 minutes at a speed of 600 rpm using a spin-coating device, the membrane was briefly dried in the ambient air. The ideal membrane had a thickness of around 4–6 μm, influenced by the solutes and the volume of solvent used during the membrane creation process. In every experiment, the control membrane shared the same composition as the experimental membranes, with the exception of not containing APASA.

Procedure

The membrane sensor was carefully placed into the spectrophotometer cuvette, which was pre-filled with 2.0 mL of borate buffer solution at pH 8.25. Subsequently, a solution with Y^{3+} ions at a specific concentration was added, and the absorbance spectrum was recorded from 350 to 750 nm at 10 nm intervals, using a control membrane as a reference. All evaluations were carried out at a temperature of 25 ± 2.0 °C. The calibration graph was created by plotting the absorbance readings acquired from various standard solutions with varying Y^{3+} ion concentrations. This graph was then employed to determine the Y^{3+} ion concentration in the sample. For membrane regeneration, it was subjected to a 2.0 minutes process in a 0.15 M nitric acid solution, ensuring its preparedness for subsequent utilization. The proposed procedure for the complexation between Y^{3+} and APASA is depicted in Scheme 1.

Safety precautions

Due to the highly toxic nature of Y^{3+} ions, all experiments involving their handling were conducted while wearing gloves. Any experimental residue containing Y^{3+} ions was meticulously gathered for proper disposal to avoid environmental pollution.

Methodology for yttrium detection in nickel-based alloys

Placing 0.5 g of nickel-based alloy in a 100 mL beaker, a blend of HCl and HNO_3 (in a ratio of 3 : 1) amounting to 16 mL was introduced to dissolve it, and the solution was heated until almost all liquid evaporated. Adding 20 mL of deionized water and 3.0 mL of 10% $H_2C_2O_4$, the beaker received further treatment. The solution's pH was adjusted to a range between 2.0 and 2.5 using ammonia solution (1 : 1). Upon adding 2.0 mL of a 10% solution of calcium chloride, a minute amount of precipitate composed of calcium oxalate was observed to form.

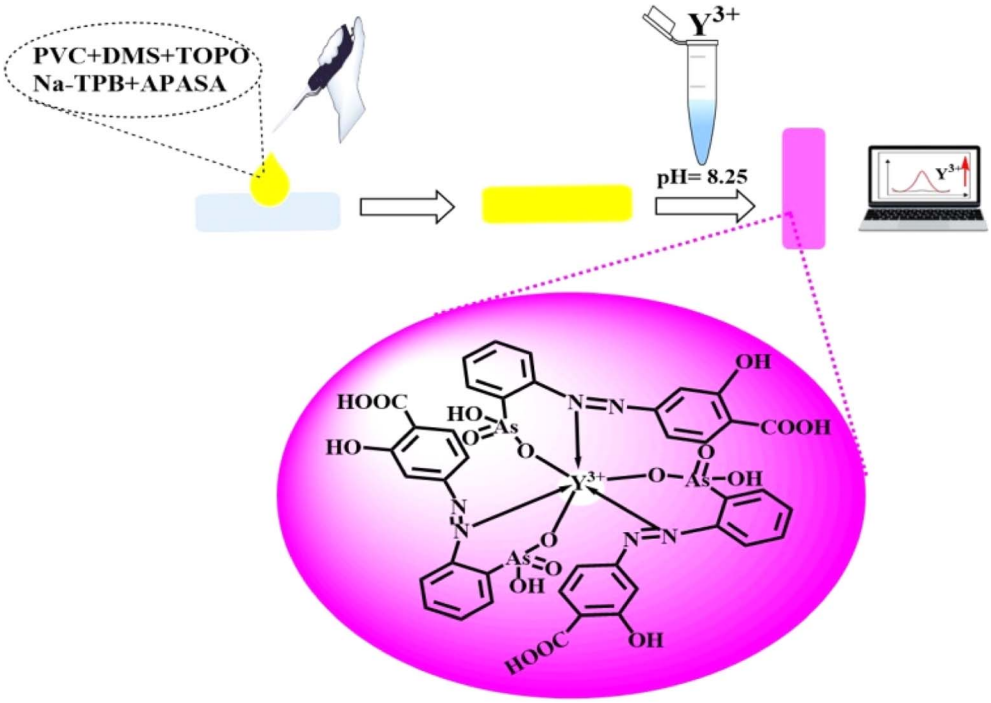

Scheme 1 Schematic representation for the preparation and complexation of Y^{3+} ions on the formed optical sensor. The images are real photos of the sensor.

As the solution's pH rose to 4.0, additional solid material precipitated within the solution. Subsequently, the solution underwent filtration, and the particulate matter was washed with water. The solid substance was then dissolved from the filter medium using 2.0 mL of a hydrochloric acid solution diluted in a 1 : 10 ratio, and the resulting liquid was collected in a 50 mL container and adjusted to the appropriate volume. Following this, 2.0 mL of sample solution labeled A-s-81, and/or 5.0 mL of sample solution labeled A-s-82, were transferred into a 25 mL calibrated flask, and the aforementioned procedure was reiterated accordingly.

Analysis of serum samples and real water

Specimens of river water gathered from Benha and tap water acquired from our laboratory were placed in centrifugation at a speed of 14 000 rotations per minute for a period of 30 minutes. After centrifuging, the resulting liquid above the sediment was employed for examination. Fetal bovine serum obtained from Sigma-Aldrich in the United States was filtered using syringe filters containing a 0.22 μm membrane. The specimens were then kept in a fridge and promptly supplemented with standard Y^{3+} solutions of different strengths. These augmented specimens were analyzed using the method described earlier and employing ICP-MS methodologies.

Results and discussion

Spectral characteristics

4-(2-Arsonophenylazo)salicylic acid (APASA) serves as a complexometric agent for zinc detection.[56] Its affinity for zinc ions can be achieved or enhanced through the use of a sensor membrane.[56] The sensor relies on a bulk equilibrium process,

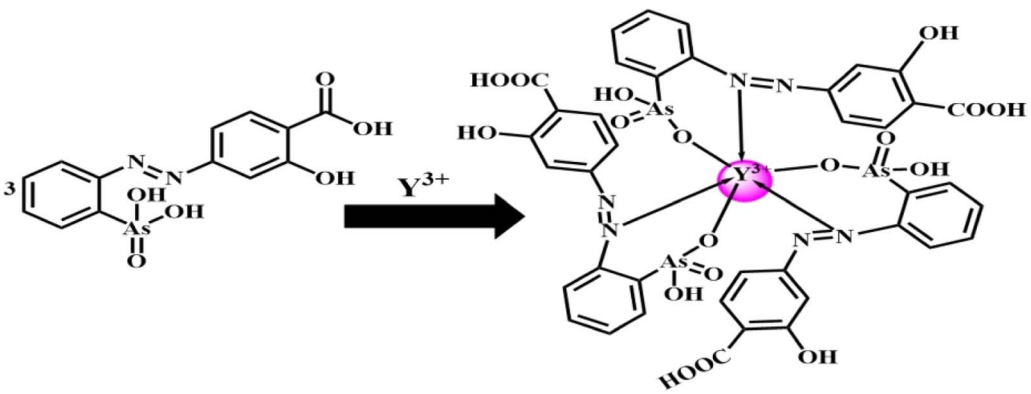

Scheme 2 Representation for the stoichiometric ratio of the formed Y^{3+}–APASA complex.

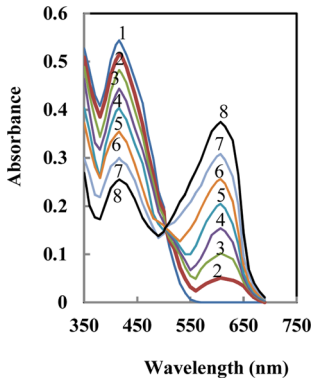

Fig. 1 Absorbance spectra of APASA membrane in the presence of increasing [Y^{3+}] ion. The numbers show the direction of absorbance changes by increasing Y^{3+}.

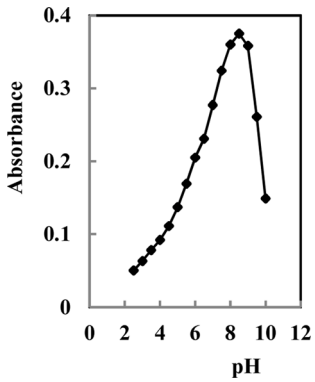

Fig. 2 Effect of pH on the response of the proposed sensor; conditions: [Y^{3+}] = 2.5 $\times 10^{-7}$ M, membrane cocktail contained 30 mg PVC, 60 mg DMS, 4.0 mg APASA, 2.0 mg TOPO and 3.0 mg Na-TPB.

where the plasticized PVC membrane's organic phase balances with the aqueous solution it contacts. In this setup, APASA functions as both an ionophore and a chromoionophore. When Y^{3+} ions permeate the membrane, they form a complex with APASA, causing an alteration in the optical properties of the membrane. The complexation between Y^{3+} ions and APASA has been analyzed in solution using techniques such as continuous variation and molar ratios. The analysis showed that APASA and Y^{3+} ions form a 3 : 1 complex, causing APASA to undergo deprotonation and release protons into the solution. The suggested structure of the complex was postulated as represented in Scheme 2. The absorption patterns of the membrane, subsequent to reaching equilibrium in a borate buffer at pH 8.25 with varying Y^{3+} ion concentrations, are illustrated in Fig. 1. As anticipated, the absorption of the unattached ligand diminishes (λ_{max} = 416 nm), while the absorption of the ligand-Y^{3+} compound amplifies (λ_{max} = 607 nm) upon the introduction of Y^{3+} ions. The presence of a distinctive isosbestic point at 503 nm additionally bolsters the formation of the Y^{3+}–APASA compound.

Impact of pH on the sensor's performance

The interaction between various reagents and metal ions relies on the solution's pH, as it influences the deprotonation or protonation of the reagent at specific pH values.[57] Various buffer media was demonstrated to assess the membrane sensor response. Universal thiel phosphate, borate, and acetate buffers were tried and studied. The favorable buffer was borate buffer solution. Fig. 2 illustrates how pH levels impact the membrane performance. Absorbance was recorded at 607 nm for 2.5 $\times$ 10^{-7} M Y^{3+} ions across a range of pH values, using a reference membrane prepared identically but without Y^{3+}. The peak performance was noted approximately at pH 8.25. Past pH 9.0, the efficacy decreases, possibly as a result of the hydrolysis of Y^{3+} ions in water, resulting in the generation of different insoluble hydroxide forms of Y^{3+}.[58] Consequently, examining the effects of pH in extremely alkaline conditions was not viable, as Y^{3+} ions precipitated under such circumstances. At acidic pH levels, the diminished sensor response is probably because hydrogen ions vie with Y^{3+} ions for APASA binding.[59]

Influence of membrane formulations

The selectivity and sensitivity attained with a particular ionophore are widely recognized to be significantly impacted by the solvent mediator, membrane composition, and additives utilized.[48] Therefore, the impact of plasticizer type, ionophore quantity, TOPO concentration, and NaTPB content as a lipophilic additive (anionic site) on the membrane sensor's responsiveness characteristics were examined.

Table 1 Effect of various plasticizers on the response of the sensors with different composition

Membrane	APASA (mg)	PVC (mg)	Plasticizer (60 mg)	TOPO (mg)	Na-TPB (mg)	Absorbance[a]
1	4.0	30	*o*-NPOE	—	—	0.086
2	4.0	30	DES	—	—	0.048
3	4.0	30	DBP	—	—	0.074
4	4.0	30	DMS	—	—	0.106
5	4.0	30	*o*-NPOE	4.0	2.0	0.139
6	4.0	30	DES	4.0	2.0	0.097
7	4.0	30	DBP	4.0	2.0	0.124
8	4.0	30	DMS	4.0	2.0	0.375

[a] Measured absorbance were recorded from a solution 2.5 $\times$ 10^{-7} M of Y^{3+} ion (pH 8.25).

Selection of plasticizer

For ensuring a consistent organic layer in the sensor membrane, the solvent (plasticizer) employed should possess chemical compatibility with the polymer used in sensor production. In this investigation, DES, DBP, *o*-NPOE, and DMS were assessed as candidate plasticizers with varying polar characteristics. The membrane sensor containing *o*-NPOE displayed insufficient physical attributes, indicating that this solvent does not possess the ideal plasticizing qualities for the current membrane sensor. Among the three remaining plasticizers examined, DMS demonstrated superior traits for the resultant membrane sensor (Table 1), leading to its adoption for further examinations. Absorbance assessments for the membrane sensor employing different plasticizer variants were carried out using a concentration of 2.5×10^{-7} M Y^{3+}, with a control membrane prepared identically but devoid of Y^{3+} ions.

Effect of APASA

In this investigation, APASA fulfills a twofold function as both an ionophore and chromoionophore, highlighting the significance of fine-tuning its amount in the formulation of the membrane sensor. Measurements of absorbance were carried out at 607 nm for membranes containing different concentrations of APASA, using a Y^{3+} ion concentration of 2.5×10^{-7} M as the standard. The blank refers to a membrane without APASA in borate buffer solution at pH 8.25. Increasing the APASA amount up to 4.0 mg led to a rise in absorbance readings (Table 2, membranes 1–4). However, higher APASA levels (surpassing 4.0 mg) did not enhance sensitivity and were deemed unsuitable because of leakage of APASA.

Impact of Na-TPB and TOPO

The synergistic phenomenon, widely utilized in solvent extraction setups, refers to the enhanced efficiency in extracting a metal ion when two reagents are combined compared to their individual performance.[57] A common form of cooperative extraction entails the retrieval of a metal ion, referred to as M^{n+}, by employing both an acidic chelating substance, HR, and a neutral alkaline agent, S. The cooperative interaction between the substances becomes notably crucial when the metal ion's coordination ability is not entirely utilized in the MRn complex. In such instances, introducing the extractant S creates a composite complex, MRnSx, which demonstrates significantly superior extraction effectiveness compared to the initial complex. To extend this principle to the envisioned membrane sensor, a study was commenced to examine the influence of TOPO on the sensor's operation.

Table 2 illustrates the composition of different manufactured membranes, with the objective of elucidating the impact of membrane formulation on resulting response attributes. Contrasting sensor membranes 5 and 6 suggests that incorporating TOPO into the membrane blend decreases the response time of the produced membrane. This can be attributed to the synergistic effect of TOPO on the interaction of Y^{3+} with APASA, which facilitates the extraction of Y^{3+} ions to the membrane sensor and their subsequent complexation. Moreover, the presence of TOPO accelerates the rate of the formation of complex, likely due to the formation of an adduct complex involving APASA, TOPO, and Y^{3+} ions, which may have a faster formation rate than the APASA-Y complex. Conversely, incorporating Na-TPB into the membrane sensor without TOPO (membrane 7 in Table 2) does not significantly improve the membrane's response time. This indicates that although Na-TPB serves as a catalyst for phase transfer and facilitates the extraction of metal ions such as Y^{3+} into the membrane sensor, the rate-determining step for response time is the complex formation between APASA and Y^{3+} ions, rather than the diffusion of Y^{3+} ions into the membrane.

Table 2 Effect of membrane composition on the response characteristic of the proposed optode

Membrane	APASA (mg)	TOPO (mg)	Na-TPB (mg)	PVC/DMS (mg/mg)	Response time (min)	Absorbance[a]
1	2.0	4.0	4.0	30/60	5.0	0.187
2	3.0	4.0	3.0	30/60	5.0	0.252
3	4.0	4.0	2.0	30/60	5.0	0.375
4	5.0	4.0	1.0	30/60	5.0	0.102
5	10.0	—	—	30/60	25	0.332
6	4.0	6.0	—	30/60	12	0.335
7	4.0	—	6.0	30/60	18	0.196
8[b]	4.0	4.0	2.0	30/60	5.0	0.375
9	4.0	3.5	2.5	30/60	7.0	0.325
10	4.0	3.0	3.0	30/60	9.0	0.284
11	4.0	2.5	3.5	30/60	10	0.246
12	4.0	2.0	4.0	30/60	13	0.209
13	4.0	5.0	1.0	30/60	10	0.327
14	4.0	4.5	1.5	28/56	8.0	0.348
15	4.0	4.0	2.0	28/56	5.0	0.375
16	4.0	3.5	2.5	28/56	7.0	0.325
17	4.0	3.0	3.0	28/56	9.0	0.283

[a] Measured absorbance were recorded from a solution 2.5×10^{-7} M of Y^{3+} ion (pH 8.25). [b] Optimum composition.

With TOPO present, Na-TPB diminishes the responsiveness time by accelerating the diffusion rate of Y^{3+} ions into the membrane sensor (upon comparing membranes 13–17 in Table 2). This implies that when TOPO is present, the diffusion of Y^{3+} ions into the membrane becomes the rate-controlling step. Essentially, the introduction of Na-TPB intensifies the diffusion rate of Y^{3+} ions into the membrane sensor. To optimize both absorption change and response time, the quantities of TOPO and Na-TPB were fine-tuned accordingly (as shown in Table 2). It's apparent from this information that the sensor membrane comprising 4.0 mg APASA, 2.0 mg Na-TPB, 30 mg PVC, 60 mg *o*-NPOE, and 4.0 mg TOPO exhibits optimal response attributes. However, it's essential to emphasize that an abundance of Na-TPB could result in reagent seepage into the sample solution.

Temperature influence

The work delved into the impact of temperature on sensing performance. Absorption spectra were meticulously recorded across a temperature range spanning from 25 to 60 °C, with the focal point being 607 nm. Notably, an increase in the Y^{3+} sample's temperature correlated with a reduction in absorbance at λ_{max}. This phenomenon is attributed to a decrease in complex formation with the membrane, a consequence of heightened ion lattice vibrations, and thermal quenching.[60] Moreover, it was observed that raising the temperature to ≥60 °C did not yield any notable variation in λ_{max} or absorbance, signifying the absence of complex formation between Y^{3+} and APASA. Consequently, the optimal temperature to obtain highly sensitive and selective results was identified as 25 ± 2.0 °C. Furthermore, the creation of a top-tier sensor was contingent upon several factors, including membrane composition adjustments, maintaining room temperature at 25 °C, controlling room humidity, and allowing the casting solution to evaporate for a duration of two days instead of one. These insights underscore the significant influence of external variables, such as temperature and humidity, on sensor preparation methodologies. It is noteworthy that the physical appearance of the sensor remained unaltered even when stored in a sealed bag for ten days.

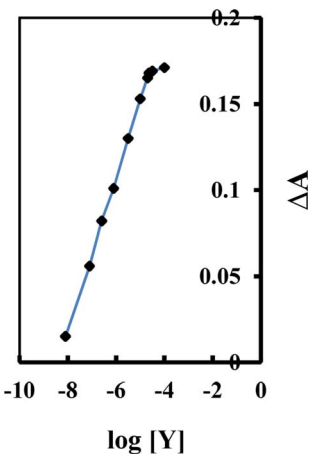

Fig. 3 Calibration curve plot for Y^{3+} sensor at 607 nm, under the optimized conditions.

Analytical figures of merit

Dynamic range and detection limit. In Fig. 3, the depicted graph illustrates the absorbance variations of the sensor presented across a range of Y^{3+} ion concentrations. The graph reveals a linear correlation between absorbance and Y^{3+} ion concentration, spanning from 8.0×10^{-9} to 2.3×10^{-5} M, with the equation $Y = 328.7X + 0.06$ ($R^2 = 0.9975$), where Y signifies absorbance and X represents Y^{3+} ion concentration in M. The sensor's determination and detection limits, defined as the analyte concentration yielding a signal equal to the blank signal plus ten and three times the blank signal's standard deviation, respectively, were determined to be 7.7×10^{-9} and 2.3×10^{-9} M, correspondingly.

Sensor's stability and response time. In the sensor constructed using the optimal composition, the response time is determined by the time required for the analyte to travel from the bulk solution to the sensor membrane interface for interaction with APASA. The assessment of response time involved monitoring the alteration in absorbance as the solution transitioned from a borate buffer solution with a pH of 8.25 to a buffered solution containing 2.5×10^{-7} M Y^{3+} ions. The duration for the sensor membrane to achieve 97% of the overall absorbance was found to be roughly 4.4 minutes for the highest concentration solution and 5.5 minutes for the most diluted solution. The sensor demonstrated stability in aq. solutions with pH < 8.25 for at least 12 hours. Throughout the initial 12 hours immersion in a borate buffer solution with a pH of 8.25, the standard deviation for $n = 12$ absorbance readings (recorded every 1 hour) of the membrane was determined to be 0.75%. This indicates the absence of any APASA seepage during this timeframe. No alteration in absorbance was noted when the sensor was exposed to light, and the membrane retained stability throughout the experiment without any APASA leakage. The membrane sensor remained unchanged for a duration of 15 days when idle and stored in ambient air.

Regeneration of the sensor. The sensor's absorbance failed to completely revert when shifting from high to low concentrations of Y^{3+} ions. Various compounds, including HNO_3, HCl, H_2SO_4, NaOH, and EDTA, were evaluated for regenerating

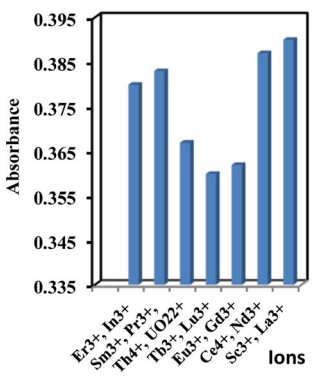

Fig. 4 Effect of 4000 TR of Sc^{3+}, La^{3+}, Sm^{3+}, Pr^{3+}, Tb^{3+}, Lu^{3+}, Eu^{3+}, Er^{3+}, Gd^{3+}, Ce^{3+}, Nd^{3+}, In^{3+}, Th^{4+}, and UO_2^{2+} on the absorbance of 2.5×10^{-7} M Y^{3+} ions using the proposed sensor at the optimum conditions.

Table 3 Tolerance ratio (TR = ion/Y^{3+} mass ratio) for various interfering ions in the determination of 2.5×10^{-7} M of Y^{3+}

Ion	TR	Ion	TR
Na^+, K^+, BO_3^-	15 000	Al^{3+}, Fe^{3+}, CO_3^{2-}	4000
Li^+, Ag^+, Tl^+, borax	13 500	Sc^{3+}, oxalate	3500
Ca^{2+}, Mg^{2+}, acetate	12 000	Pd^{2+}, Ni^{2+}, SO_4^{2-}	3000
Sr^{2+}, Ba^{2+}, NO_2^-, PO_4^{3-}	10 000	Hg^{2+}, Co^{2+}, HCO_3^{2-}	2600
Ge^{4+}, Ti^{4+}, NO_3^-	9000	Pb^{2+}, Sn^{2+}, Cl^-	2250
Sm^{3+}, Pr^{3+}, IO_3^-	7500	Pt^{4+}, Sn^{4+}, SCN^-	2000
Eu^{3+}, Gd^{3+}, $S_2O_3^{2-}$	6500	Au^{3+}, La^{3+}, Cr^{3+}	1500
Er^{3+}, Lu^{3+}, Br^-	5000	Se^{4+}, Te^{4+}	1000
Th^{4+}, UO_2^{2+}, $B_4O_7^{2-}$	4500	Cd^{2+}, Zn^{2+}, In^{3+}	750

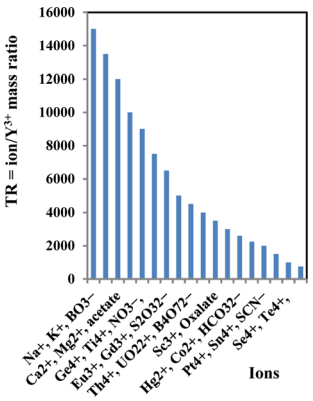

Fig. 5 Tolerance ratio for various interfering ions in the determination of 2.5×10^{-7} M of Y^{3+}.

sensors immersed in Y^{3+} solutions. Out of all the compounds tested, 0.15 M HNO_3 was found to completely regenerate the sensor within 3.0 minutes. It's crucial to emphasize that following the restoration process, and prior to undertaking additional examinations, the membrane should be submerged in a borate buffer solution at pH 8.25 for a minimum of 3.0 minutes.

Reproducibility and repeatability. The repeatability and reproducibility of the sensor are key attributes. The repeatability of the sensor membrane was assessed by repeatedly immersing the sensor in solutions containing 2.5×10^{-7} M Y^{3+} ions and a 0.15 M HNO_3 solution. The relative standard deviation of the recorded absorbance values (at $\lambda = 607$ nm) in the Y^{3+} solution stood at approximately 2.16% for ten measurements, indicating the repeatability of the sensor's response. The reproducibility of various sensor membranes was gauged by measuring absorbance from a 2.5×10^{-7} M Y^{3+} solution across six sensor membranes, with the relative standard deviation of the recorded absorbance values (at $\lambda = 607$ nm) in the Y^{3+} ions solution found to be approximately 2.93%. These findings affirm that the repeatability and reproducibility of the presented sensor membrane are commendable.

Selectivity. Arguably the most crucial characteristics of the provided sensor membrane lie in its selectivity, which signifies its preference for the primary ion over various other ions present in the solution. Hence, an investigation was conducted to assess the impact of numerous common lanthanides and transition metal ions on the absorbance of the proposed Y^{3+} sensor. To assess the selectivity of the proposed Y^{3+} sensor, the absorbance of a fixed level of Y^{3+} ion, at 2.5×10^{-7} M, in a solution of pH 8.25 was measured before (A_o) and after (A) addition of some potentially interfering ions such as Sm^{3+}, Pr^{3+}, Eu^{3+}, Gd^{3+}, Er^{3+}, Lu^{3+}, La^{3+}, Sc^{3+}, Hg^{2+}, Cu^{2+}, Mn^{2+}, Zn^{2+}, Ni^{2+}, Co^{2+}, Sr^{2+}, Au^{3+}, Al^{3+}, and Fe^{3+} at concentrations up to 750 times of the analyte ion. The resulting relative error is defined as $RE(\%) = [(A - A_o)/A_o] \times 100$. Although rare earth elements

Table 4 Comparison between the proposed procedure with the recent literature for Y^{3+} ion determination

Reagent	Conditions	λ_{max}, nm	ε_{max}, L mol^{-1} cm^{-1}	M : L	Linear range, μg mL^{-1}	Interfering ions	Ref.
p-Nitrochlorophosphonazo	0.2–0.5 M $HClO_4$	731	8.49×10^4	1 : 3	0.0–6.0	La^{3+}, Ce^{4+}, Pr^{3+}, Nd^{3+}, Sm^{3+}, Eu^{3+}, Gd^{3+}	61
Eriochrome cyanine R	3% HCl	650	—	—	0.2–3.0	Th^{4+}, UO_2^{2+} La^{3+},Co^{2+}, Cu^{2+}, Ni^{2+}, Cr^{3+}, Sc^{3+}	5
5-(4-chlorophenylazo)-6-hydroxypyrimidine-2,4-dione	0.1–1.4 M HCl	610	1.60×10^4	1 : 1, 1 : 2	0.2–3.2	Zn^{2+}, Cu^{2+}, La^{3+}, Sc^{3+}, Eu^{3+},Gd^{3+}	62
Arsenazo III	pH 2.3 to 2.7	660	1.4×10^3	1 : 1	0–50	Fe^{2+}, Cr^{6+}, Fe^{3+}, $S_2O_3^{2-}$, CH_4N_2S	63
Alizarin red S	pH 4.7	520	1.16×10^4	—	0.13–3.73	V^{5+}, Al^{3+}, Fe^{2+}, Co^{2+}, Ce^{4+}, Ti^{4+}, PO_4^{3-}	64
Chlortetracycline (CTC)-silver nanoparticles (AgNPs)	pH 7.3	540	—	1 : 1	18–243 nM	La^{3+}, Tb^{3+}, Sm^{3+}, Gd^{3+}, Pr^{3+}, Nd^{3+}, Er^{3+}, Tm^{3+}	14
Arsenazo I	pH 5.6	570	—	1 : 1	0.04–0.4	La^{3+}, Sm^{3+}, Gd^{3+}, Pr^{3+}, Nd^{3+}, Er^{3+}	65
Alizarin red S and trioctylphosphine oxide	pH 4.9	519	0.53×10^4	—	1.0–26	Bi^{3+}, Th^{4+}, PO_4^{3-}, La^{3+}, Sn^{2+}	36
Dibenzo-18-crown-6	pH = 9.0	280	1.35×10^4	—	0.8–16.2	Th^{4+}, UO_2^{2+} La^{3+}	37
1,6-bi(10-phenyl-30-methyl-50-pyrazolone-40-hexanedione)	pH = 5.0–6.1	467	—	1 : 2	0.0009–0.9	Sm^{3+}, Nd^{3+}, Er^{3+}, Eu^{3+}, Tm^{3+}, Tb^{3+}, Sc^{3+}, Pr^{3+}, Dy^{3+}, Gd^{3+}, La^{3+}, Lu^{3+}	66
Xylenol orange	pH = 5.0	568	3.4×10^4	1 : 1	0.2–6.0	La^{3+}, Ce^{3+}, Pr^{3+}, Nd^{3+}, Sm^{3+}, Eu^{3+}, Gd^{3+}, Tm^{3+}, Yb^{3+}, Tb^{3+}, Lu^{3+}	38
APASA membrane	pH = 8.25	607	3.23×10^7	1 : 3	8.0×10^{-9}–2.3×10^{-5}	In^{3+}	This work

Table 5 Determination of yttrium in nickel-base alloys

	Reference value, %		Y found[c], %					
Sample no.	Ce[b]	Y	Proposed	ICP-MS	Recovery, %	RSD, %	*t*-test[a]	*F*-value[a]
NBA-1	0.16	—	0.013	0.025	101.30	2.25	1.83	3.67
NBA-2	0.10	0.047	0.048	0.50	102.13	1.33	2.05	4.12
NBA-3	0.04	—	0.001	0.005	102.50	1.61	1.58	3.44
NBA-4	0.19	0.17	0.166	0.178	97.65	2.37	2.16	4.39
A-s-81	—	0.046	0.0453	0.050	98.48	2.15	1.70	3.56
A-s-82	—	0.01	0.0097	0.0107	97.00	1.88	1.94	3.85

[a] Theoretical values for *t* and *F* at 95% confidence limit are 2.57 and 5.05, respectively. [b] Cerium sub-group rare earths. [c] Average of six replicate measurements ± standard deviation.

exhibit very similar properties, it has a negligible effect on yttrium absorbance using the proposed sensor at the optimum conditions (Fig. 4). The data clearly demonstrate that, across all the examined metal ions, the relative error remains below 4.0%, a level considered acceptable. As shown in Fig. 4, La^{3+}, Sc^{3+}, Lu^{3+}, Nd^{3+}, Sm^{3+}, Pr^{3+}, Er^{3+}, In^{3+} has slightly positive interference, whereas a negligible negative interference of Eu^{3+}, Gd^{3+}, Tb^{3+}, Lu^{3+}, Th^{4+}, and UO_2^{2+} was achieved. Further investigation revealed that anions like NO_3^-, $C_2O_4^{2-}$, CO_3^{2-}, NO_2^-, BO_3^-, IO_3^-, and borax, even at elevated concentrations up to 2000 times, did not exhibit significant interference with the Y^{3+} assay (see Table 3 and Fig. 5). These findings suggest that the presented sensor exhibits high selectivity towards Y^{3+} ions and can effectively detect traces of Y^{3+} ions in natural biological and environmental samples, even in the presence of numerous other co-existing cationic and anionic species. Additionally, the proposed sensor offers the benefits of a short response time and applicability over a wider concentration range.

The effectiveness of the suggested sensor membrane was contrasted with a selection of prior spectrophotometric methods[5,14,36,38,61–66] (Table 4). Notably, the proposed sensor membrane stands out for its rapid response time and suitability across a broad concentration spectrum. Demonstrating selectivity towards Y^{3+} ions over transition and lanthanide ions, this sensor membrane meets the requisite selectivity coefficients essential for detecting Y^{3+} ions in groundwater, food, and biological samples.

Analytical applications

Identification of Y^{3+} in nickel-based alloys. To validate the effectiveness of the proposed technique, it was utilized to detect Y^{3+} in nickel-based alloys. Yttrium content in six alloy samples, namely NBA-1, NBA-2, NBA-3, NBA-4, A-s-81, and A-s-82, was examined and quantified. The analytical parameters established through standard investigations for the proposed approach were applied to analyze the results. Table 5 illustrates

Table 6 Determination of Y^{3+} in water samples

		Found[a] (ng mL^{-1}) ± SD				
Sample	Spiked ng mL^{-1}	Proposed	ICP-MS	Recovery, %	*t*-test[b]	*F*-value[b]
Tap water	20	20.5 ± 0.27	19.2 ± 1.43	102.5	1.68	
	40	39.4 ± 0.18	40.8 ± 1.73	98.5		3.31
	60	59.0 ± 0.29	61.1 ± 1.50	98.3	1.46	
	50	48.9 ± 0.21	51.2 ± 1.62	97.8	1.75	
Mineral water	100	101.0 ± 0.26	98.2 ± 1.38	101.0		3.23
	200	197.2 ± 0.19	204.7 ± 1.15	98.6	1.24	
Well water	30	30.3 ± 0.31	29.2 ± 1.37	101.0	1.37	
	60	61.5 ± 0.25	59.0 ± 1.53	102.5		3.14
	90	88.8 ± 0.21	91.1 ± 1.31	98.7	1.56	
Red sea water	40	40.5 ± 0.27	39.3 ± 0.96	101.2		3.44
	80	79.0 ± 0.33	81.2 ± 1.56	98.8	1.85	
	160	157.5 ± 0.37	162.5 ± 1.44	98.4		3.76
Mediter-ranean sea water	60	58.9 ± 0.31	61.0 ± 1.21	98.2	1.72	
	120	122.0 ± 0.34	117.4 ± 1.17	101.7		3.59
	240	235.7 ± 0.22	246.2 ± 0.95	98.2	1.64	
Industrial water	70	69.0 ± 0.12	71.2 ± 1.04	98.6		3.68
	140	141.6 ± 0.51	137.5 ± 1.72	101.1	1.83	
	210	214.8 ± 0.38	224.6 ± 1.47	102.3		3.55

[a] Average of six replicate determinations ± standard deviation. [b] Theoretical values for *t* and *F* at 95% confidence limit are 2.57 and 5.05, respectively.

the experimental findings for the alloy samples, indicating relative standard deviations (RSDs) below 2.4%. Recoveries calculated for the water samples ranged from 97.0% to 102.5%.

Assessing performance entailed computing the *F*-test (for precision) and *t*-value (for accuracy) when compared to the ICP-MS technique. Mean values were ascertained using Student's *t*- and *F*-tests at a 95% confidence level, accounting for five degrees of freedom.[67] Findings revealed that the computed values did not exceed the expected values, indicating no notable deviation from the reference method.

Identification of Y^{3+} in real water samples. Yttrium, classified as a heavy rare-earth element, finds extensive application across various contemporary industrial sectors, including alloy production, optical glass manufacturing, ceramics, and nuclear energy.[68] However, recent findings have indicated elevated Y^{3+} levels in urine and drinking water near mining sites. Prolonged exposure to Y^{3+} poses significant health risks and warrants considerable concern.[69] To assess the practical utility of our developed sensing approach, we subjected the membrane to testing with actual samples. The levels of Y^{3+} contamination in these samples were either below, approximately equal to, or higher than the proposed sensor's limit of detection (25, 50, and 100 nM) (Table 6). The consistent colorimetric response observed in both pure and real water samples indicates the sensor's resilience against interference from contaminants present in real water samples. Thus, these findings validate the efficacy of the developed sensor for Y^{3+} ion determination in real water samples. The sensor offers advantages such as a short response time (within 5.0 min), a low detection limit at the nanomolar level, operation at physiological pH (pH 8.25), and suitability for real water samples, distinguishing it from other methods. Application of the proposed sensor in analyzing spiked samples, including real water samples from various sources and fetal bovine serum, yielded valuable and plausible results, as previously reported.[39] Additionally, a comparative assessment of our sensor's analytical performance against that of ICP-MS methods was conducted. The proposed sensor membrane exhibited superior performance in terms of ultra-sensitivity, rapid response, exceptional specificity, user-friendly operation, and application efficiency (Table 6). These findings underscore the broad potential applications of our sensor in analyzing complex environmental and biological samples.

Conclusion

The proposed approach offers a sensitive, precise, cost-effective, and selective method for Y^{3+} ion determination, leveraging an optical sensor membrane. The novelty of the proposed sensor is to is to prepare a plasticized PVC membrane immobilizing 4-(2-arsonophenylazo)salicylic acid (APASA) and employed to craft an ion-selective sensor aimed to determine Y^{3+} ions. The main challenge faced was the slow reaction rate between Y^{3+} and APASA. Overcoming this hurdle involved introducing an additional reagent, such as tri-*n*-octyl phosphine oxide (TOPO), to enhance the complexation of Y^{3+} by APASA within the membrane. Within the sensor membrane, APASA functions dually as an ionophore and chromoionophore, while TOPO enhances the complexation of APASA with Y^{3+} ions synergistically. Upon interaction with Y^{3+} ions, the membrane sensor undergoes a reversible color change from yellow to violet. Notably, the optical sensor exhibits strong selectivity for Y^{3+} over other lanthanide ions. The investigation into the composition of the sensor membrane aimed to achieve a (1 : 3) (M : L) complex formation. The linear detection range of the developed sensor membrane spans from 8.0×10^{-9} to 2.3×10^{-5} M of Y^{3+} ions, with detection and quantification limits of 2.3×10^{-9} and 7.7×10^{-9} M, respectively. These findings affirm the potential of the sensor membrane for routine analysis using portable equipment. Comparing the proposed optode with previously reported spectrophotometric methods for Y^{3+} (Table 4) indicates comparable properties. The sensor membrane demonstrates stability and reliability, making it suitable for applications in environmental and biological samples.

Data availability

All data are available as it is required.

Author contributions

Mahmood Aljabri and Salah El-Bahyi: conceptualization, investigation, data curation, visualization, methodology, validation, writing – original draft, writing – review & editing. Refat El-Sayed and Khaled Debbabi: data curation, conceptualization, methodology, validation, investigation, visualization, writing – original draft & editing. Alaa Amin: conceptualization, supervision, validation, methodology, investigation, writing – original draft, writing – review & editing.

Conflicts of interest

The authors declare that they have no known competing financial interests or personal relationships that could have appeared to influence the work reported in this paper.

Acknowledgements

The authors extend their appreciation to Taif University, Saudi Arabia for supporting this work through project number (TU-DSPP-2024-20).

References

1 B. Fu, J. C. Hower, W. Zhang, G. Luo, H. Hu and H. Yao, *Prog. Energy Combust. Sci.*, 2022, **88**, 100954.
2 Z. H. Zhu and A. R. Zheng, *Molecules*, 2018, **23**, 489–501.
3 S. N. Wang, S. Liu, J. Y. Zhang and Y. Cao, *Talanta*, 2019, **198**, 501–509.
4 K. Okamoto and S. J. Fukuzumi, *J. Am. Chem. Soc.*, 2004, **126**, 13922–13923.
5 A. M. Abdallah, M. A. Kabil, A. Ismael and D. S. Akl, *J. Iran. Chem. Soc.*, 2004, **1**, 79–87.

6 D. Paderni, L. Giorgi, V. Fusi, M. Formica, G. Ambrosi and M. Micheloni, *Coord. Chem. Rev.*, 2021, **429**, 213639–213657.
7 Y. Y. Chang, B. W. Liu, Z. C. Huang, Y. B. Liu, M. Liu and J. W. Liu, *Langmuir*, 2020, **36**, 1034–1042.
8 T. Zako, M. Yoshimoto, H. Hyodo, H. Kishimoto, M. Ito, K. Kaneko, K. Soga and M. Maeda, *Biomater. Sci.*, 2015, **3**, 59–64.
9 A. Assy, H. J. Lin, M. Schoenauer-Sebag, P. Gredin, M. Mortier, L. Billot, Z. Chen and L. Aigouy, *Sens. Actuators, A*, 2016, **250**, 71–77.
10 M. A. Hernandez-Rodriguez, A. D. Lozano-Gorrin, V. Lavin, R. U. R. Mendoza and I. R. Martin, *Opt. Express*, 2017, **25**, 27845–27856.
11 Y. Qi, F. Zhao, X. M. Xie, X. Q. Xu and Z. Y. Ma, *Spectrosc. Lett.*, 2014, **48**, 311–316.
12 C. H. Yeong, M. H. Cheng and K. H. Ng, *J. Zhejiang Univ. Sci. B*, 2014, **15**, 845–863.
13 W. D. Yang, P. Zhang, J. S. Liu and Y. F. Xue, *J. Rare Earths*, 2006, **24**, 369–373.
14 G. Ghodake, S. Shinde, R. G. Saratale, A. Kadam, G. D. Saratale and D. Y. Kim, *Colloids Surf., B*, 2019, **183**, 110436–110442.
15 S. Ilyas, H. Kim, R. R. Srivastava and S. Choi, *J. Cleaner Prod.*, 2021, **278**, 123435.
16 L. S. Wang, X. W. Huang, Y. Yu, L. S. Zhao, C. M. Wang, Z. Y. Feng, D. L. Cui and Z. Q. Long, *J. Cleaner Prod.*, 2017, **165**, 231–242.
17 T. C. Liu and J. Chen, *Sep. Purif. Technol.*, 2021, **276**, 119263.
18 M. K. Jha, A. Kumari, R. Panda, J. R. Kumar, K. Yoo and J. Y. Lee, *Hydrometallurgy*, 2016, **165**, 2–26.
19 D. Q. Li, *J. Rare Earths*, 2017, **35**, 107–119.
20 N. Swain and S. Mishra, *J. Cleaner Prod.*, 2019, **220**, 884–898.
21 M. Traore, A. J. Gong, Y. W. Wang, L. N. Qiu, Y. Z. Bai, W. Y. Zhao, Y. Liu, Y. Chen, Y. Liu, H. L. Wu, S. L. Li and Y. Y. You, *J. Rare Earths*, 2023, **41**, 182–189.
22 M. I. Aly, B. A. Masry, M. S. Gasser, N. A. Khalifa and J. A. Daoud, *Int. J. Miner. Process.*, 2016, **153**, 71–79.
23 D. Q. Li, *J. Rare Earths*, 2019, **37**, 468–486.
24 K. Liu, Z. K. Wang, X. M. Tang and S. Q. Lu, *Sep. Sci. Technol.*, 2016, **51**, 2804–2814.
25 G. L. Wu, Z. F. Zhang, Y. L. Li and W. P. Liao, *J. Rare Earths*, 2022, **40**, 958–964.
26 J. B. Hiskey and R. G. Copp, *Miner. Eng.*, 2018, **125**, 265–270.
27 J. G. S. Gupta, *Talanta*, 1981, **28**, 31–36.
28 E. S. Koshel, V. B. Baranovskaya and Y. Gubanova, *Inorg. Mater.*, 2016, **52**, 1449–1454.
29 G. V. Ramanaiah, *Talanta*, 1998, **46**, 533–540.
30 B. A. Wiethan, P. C. do Nascimento, A. N. Colim, A. F. Guarda, F. R. Adolfo, M. B. da Rosa, L. M. de Carvalho and D. Bohrer, *Anal. Lett.*, 2019, **52**, 2057–2068.
31 W. Cui, Z. Cai, Q. Li, H. Qu, J. Zheng, D. Yu, J. Chen and Z. Wang, *Talanta*, 2023, **255**, 124248.
32 Y. V. Franca, F. Leitgo, H. M. Shihomatsu Jr and W. S. Scapin, *Chromatographia*, 1999, **49**, 91–94.
33 C. Nan, S. Xinjian, L. bin, W. Jian, W. Jiahui, O. Aiguo and L. Yande, *Opt. Laser Technol.*, 2024, **170**, 110279.
34 M. Zadvydas, S. Tamulevicius and T. Grinys, *Mater. Sci.*, 2004, **10**, 349–352.
35 D. Zhang, Z. Zang, X. Zhou, Y. Zhou, X. Tang, R. Wei and W. Liu, *Inorg. Chem. Commun.*, 2009, **12**, 1154–1156.
36 S. A. Mohammad and S. Y. S. Zeebaree, *Sci. J. Chem.*, 2017, **5**, 80–86.
37 Y. K. Agrawal, S. K. Menon and S. Sudhakar, *Sep. Purif. Technol.*, 2001, **24**, 197–203.
38 R. M. Elrakaiby, *Al-Azhar Bull. Sci.*, 2018, **29**, 81–89.
39 M. M. Hussain, M. M. Rahman, M. N. Arshad and A. M. Asiri, *Sci. Rep.*, 2017, **7**, 5832–5843.
40 W. Thanasarakhan, S. Kruanetr, R. L. Deming, B. Liawruangrath, S. Wangkarn and S. Liawruangrath, *Talanta*, 2011, **84**, 1401–1409.
41 A. S. Amin, *Eurasian J. Anal. Chem.*, 2018, **13**, 1–12.
42 H. H. El-Feky, A. S. Amin and E. M. I. Moustafa, *RSC Adv.*, 2022, **12**, 18431–18440.
43 M. Aish, R. F. Alshehri and A. S. Amin, *RSC Adv.*, 2023, **13**, 24777–24788.
44 A. A. Gouda and A. S. Amin, *Int. J. Envir. Anal. Chem.*, 2022, **102**, 7313–7328.
45 A. S. Amin, H. H. El-Feky and N. Hassan, *RSC Adv.*, 2022, **12**, 26620–26629.
46 H. H. El-Feky, S. M. El-Bahy and A. S. Amin, *Anal. Biochem.*, 2022, **651**, 114720.
47 A. S. Amin and H. El-Feky, *Iran. J. Anal. Chem.*, 2021, **8**, 65–77.
48 H. H. El-Feky, S. M. El-Bahy, A. M. E. Hassan and A. S. Amin, *Int. J. Environ. Anal. Chem.*, 2023, **103**, 4031–4048.
49 R. F. Alshehri, M. Hemdan, A. O. Babalghith, A. S. Amin and E. R. Darwish, *RSC Adv.*, 2024, **14**, 712–724.
50 S. Parveen, A. Pathak and B. D. Gupta, *Sens. Actuators, B*, 2017, **246**, 910–919.
51 S. Wang, S. Chen, K. Shang, X. Gao and X. Wang, *Int. J. Biol. Macromol.*, 2021, **189**, 356–362.
52 R. Uzek, E. Sari and A. Merkoci, *Magnetochemistry*, 2019, **5**, 59–84.
53 J. Wang, Y. Shen, X. Li, Y. Xia and C. Yang, *Sens. Actuators, B*, 2019, **298**, 126858.
54 J. Wang, H. Lin, Y. Cheng, X. Cui, Y. Gao, Z. Ji, J. Xu and Y. Wang, *Sens. Actuators, B*, 2019, **278**, 165–171.
55 J. A. Dean, *Analytical Chemistry Handbook*, McGraw-Hill, New York, 1995, pp. 30–34.
56 R. F. Alshehri, H. H. El-Feky, A. M. Askar, A. S. Amin and M. Aish, *Spectrochim. Acta, Part A*, 2024, **305**, 123424.
57 E. B. Sandell and H. Onishi, *Photometric Determination of Traces of Metal: General Aspect*, Interscience Publishers, New York, 4th edn, 1978.
58 J. Lurie, *Handbook of Analytical Chemistry*, English translation by N. Bobrov, Moscow, 1978.
59 E. M. I. Moustafa, A. S. Amin and E. R. Darwish, *RSC Adv.*, 2022, **12**, 26090–26098.
60 K. Saidi, W. Chaabani and M. Dammak, *RSC Adv.*, 2021, **11**, 30926–30936.
61 C.-G. Hsu and J.-M. Pan, *Analyst*, 1985, **110**, 1245–1248.
62 A. S. Amin, T. Y. Mohammed and A. A. Mousa, *Spectrochim. Acta, Part A*, 2003, **59**, 2577–2584.
63 D. I. Wood and M. R. Adams, *Analyst*, 1970, **95**, 556–561.

64 S. A. Mohammad and S. Y. Zebary, *Raf. J. Sci.*, 2018, **27**, 127–137.
65 S. D. Sawnt, R. Sundaresan and P. K. Mathur, *Indian J. Chem.*, 2001, **40**, 323–326.
66 X. Wu, L. Li, J. Yang, Y. Wang, S. Sun and N. Wang, *Microchim. Acta*, 2003, **141**, 165–168.
67 J. N. Miller and J. C. Miller, *Statistics and Chemometrics for Analytical Chemistry*, Prentice-Hall, London, 5th edn, 2005.
68 A. V. Naumov, *Russ. J. Non-Ferr. Met.*, 2008, **49**, 14–22.
69 Q. Liang, H. Yin, J. Li, L. Zhang, R. Hou and S. Wang, *Medicine*, 2018, **97**, e12717.